Journal of Marine Science and Technology

Volume 26 | Issue 2 Article 10

DESIGN OF AN INTELLIGENT DAMPING CONTROLLER OF STATCOM WITH HVDC FOR LARGE OFFSHORE WIND FARM

Kai-Hung Lu
School of Information Technology, Beijing Institute of Technology, Zhuhai,China.Key Laboratory of Photoelectric Imaging Technology and System, Ministry of Education of China.

Hsin-Chuan Chen
School of Information Technology, Beijing Institute of Technology, Zhuhai,China.Key Laboratory of Photoelectric Imaging Technology and System, Ministry of Education of China.

Yu Su
School of Information Technology, Beijing Institute of Technology, Zhuhai,China.Key Laboratory of Photoelectric Imaging Technology and System, Ministry of Education of China.

Qiangqiang Xu
School of Information Technology, Beijing Institute of Technology, Zhuhai,China.Key Laboratory of Photoelectric Imaging Technology and System, Ministry of Education of China.

Recommended Citation

Lu, Kai-Hung; Chen, Hsin-Chuan; Su, Yu; and Xu, Qiangqiang (2018) "DESIGN OF AN INTELLIGENT DAMPING CONTROLLER OF STATCOM WITH HVDC FOR LARGE OFFSHORE WIND FARM," *Journal of Marine Science and Technology*: Vol. 26: Iss. 2, Article 10.
DOI: 10.6119/JMST.2018.04_(2).0010
Available at: https://jmstt.ntou.edu.tw/journal/vol26/iss2/10

Journal of Marine Science and Technology, Vol. 26, No. 2, pp. 228-239 (2018)
DOI: 10.6119/JMST.2018.04_(2).0010

DESIGN OF AN INTELLIGENT DAMPING CONTROLLER OF STATCOM WITH HVDC FOR LARGE OFFSHORE WIND FARM

Kai-Hung Lu[1, 2], Hsin-Chuan Chen[1, 2], Yu Su[1, 2], and Qiangqiang Xu[1, 2]

Key words: functional link-based recurrent fuzzy neural network (FLRFNN), genetic algorithm hybrid time varying particle swarm optimization (GAHTVPSO), offshore wind farm (OWF), Intelligent Damping Controller (IDC).

ABSTRACT

This paper proposes the design of an Intelligent Damping Controller (IDC) for a Static Synchronous Compensator (STATCOM), linking to a high voltage direct current (HVDC) transmission line, where a permanent magnet synchronous generator (PMSG)-based offshore wind farm (OWF) is connected. This IDC consists of a critic network with the proposed Functional Link based Recurrent Fuzzy Neural Network (FLRFNN) and Genetic Algorithm Hybrid Time Varying Particle Swarm Optimization (GAHTVPSO) algorithm. A single-machine infinite-bus and a multi-machine hybrid power system were used for test the system stability. GAHTVPSO approach is developed to adjust the learning rates to improve the learning capability. Analysis of the performance shows that it can achieve better damping characteristics.

I. INTRODUCTION

Wind generation systems are attracting considerable attention as clean and safe sources of renewable power (Cardenas et al., 2005). In recent years some small-scale offshore wind farms (OWFs) are evaluated, whiles a number of large-scale OWFs have been constructed and are now in commercial operation. There are also a lot of interest in PMSG, owing to their compact structure, high air-gap flux density, high power density, high torque-to-inertia ratio, and high torque capability (Lin et al., 2011). When OWFs through HVDC systems deliver a large amount of electric power to power grids, the inherent power fluctuations that occur can have adverse impacts on the power quality of the systems to which they are connected.

In recent years, the dynamic control strategies for the HVDC with STATCOM are often discussed. The STATCOM proposed by Gyugyi and Hingorani, is the most versatile and powerful FACTS device (Zhou et al., 2011a; Zhou et al., 2011b). It can increase the system security by raising the transient stability limit, limiting short circuit currents and overloads, blackouts and damping oscillations of power systems. Several studies have proposed control methods for STATCOM to improve the damping of the low frequency power oscillations, such as the use of nonlinear voltage control loops, state feedback control techniques, Phase and Amplitude Control or Adaptive critic designs (Lingling and Zhixin, 2016; Chen et al., 2010). However, the complexity of the wind farm power systems, to which the STATCOM is connected, means that the control schemes become less efficient with regard to mitigating power oscillations thus reduce the control performance. Some studies have proposed external controllers using intelligent control schemes, such as fuzzy logic controllers, neuro-fuzzy external controllers, hybrid Fuzzy/LQR controllers and a Gray-Based Genetic algorithm method (Mohagheghi et al., 2007; Hong and Luo 2009; Wang and Truong, 2013a).

This paper proposed an Intelligent Damping Controller (IDC) for a STATCOM to damp power system oscillations. The proposed IDC consists of the adaptive critic network, the functional link-based recurrent fuzzy neural network (FLRFNN) and the Genetic Algorithm Hybrid Time Varying Particle Swarm Optimization (GAHTVPSO) algorithm.

With the dynamics being continually identified by a model, the recurrent fuzzy neural networks (RFNN) is suitable for multivariable applications especially for a system with unclear and complex dynamics (Lin et al., 2010). The functional-link neural network (FLNN) is adopted for FLRFNN to improve the RFNN performance in this paper. The input variables are trigonometric basis function and the linearly independency are used for a functional expansion of the FLNN in the extended space for classification. Therefore, FLNN can approximate a nonlinear function effectively (Lin et al., 2009; George and Panda, 2012) to be applied in the system applications. The adaptive critic network is evaluated in relation to the FLRFNN

Paper submitted 12/06/16; revised 01/09/18; accepted 01/31/18. Author for correspondence: Qiangqiang Xu (e-mail: 418117603@qq.com).
[1] *School of Information Technology, Beijing Institute of Technology, Zhuhai, China.*
[2] *Key Laboratory of Photoelectric Imaging Technology and System, Ministry of Education of China.*

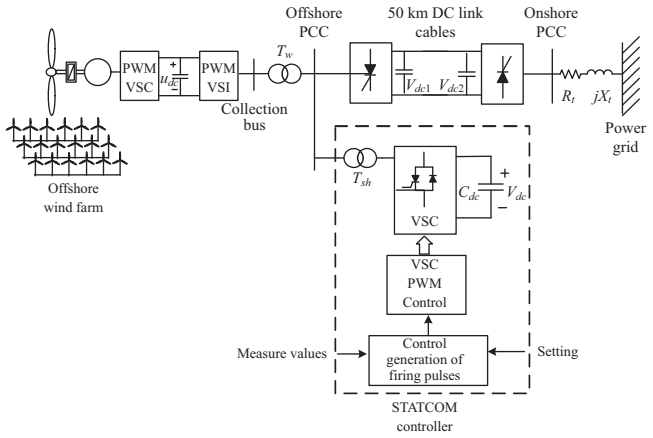

Fig. 1. Configuration of a STATCOM system with the OWF connected to power grid through an HVDC link.

controller, so the optimal damping control signal can be provided to the STATCOM.

However, the initial values of FLRFNN and the adaptive critic network learning rates are normally difficult to obtain. This paper also proposed the crossover operation to the particles' chromosome in the GAHTVPSO to find the optimal values of these learning rates. Particle swarm optimization (PSO) was first introduced by Kennedy and Eberhart in 1995 (Eberhar and Shi, 2001; Chaturvedi et al., 2008). Since it is population based and self-adaptive, it has gained increasing popularity as an efficient alternative to genetic algorithms (GAs). Moreover, PSO has been shown to be effective in optimizing difficult multidimensional continuous problems in a variety of research fields. In addition, compared with GA, PSO has the ability to remember knowledge of good solutions, and which can also be retained by all the particles involved performance, the PSO-Time Varying Acceleration Coefficients (PSO-TVAC) parameter tuning approach has recently been shown to be effective in improving the performance of PSO (Varshney et al., 2011).

II. ANALYSIS OF SYSTEM MODELS

Fig. 1 shows the configuration of the system studied in this paper. The integrated OWF is connected to a power grid through a 50 km HVDC transmission line. The OWF, represented by a large equivalent aggregated PMSG, is driven by an equivalent aggregated wind turbine through the gearbox in (Wang and Truong, 2013c). The aggregated OWF containing 100 MW PMSG-based wind turbine generators is connected to an offshore bus through a step-up transformer T_w. The voltage of the offshore PCC bus is stepped up to 24 kV. The onshore PCC bus is connected to the power grid through a transmission line with $R_t + jX_t$. The proposed STATCOM is 70 MVar, with voltage source converter (VSC) connected in shunt via a shunt transformer T_{sh}, primarily to provide the real power demand at the common DC link.

1. Wind Turbine Model

The wind turbine model based on PMSG is the mechanical power turning the generator rotor. The PMSG wind farm consists of a PWM voltage source converter and an inverter for wind power generation speed control, as illustrated in Fig. 1, the "VSC" and "VSI". The VSC and VSI voltage-oriented vector control design and control block diagram of the PMSG have been presented in (Wang and Truong, 2013b). For a variable speed wind turbine, the output mechanical power available from a wind turbine can be expressed as

$$P_m = 0.5\rho A C_p\left(\lambda, \beta\right)V_\omega^3 \tag{1}$$

where ρ and A are the air density and impact area swept by blades, respectively. V_ω is the wind velocity (m/sec), and C_p is called the power coefficient, and is given as a nonlinear function of the tip speed ratio $\lambda = \omega_r/V_\omega$. ω_r is the turbine speed of blade radius. C_p is a function of the λ and the blade pitch angle β, and is generally defined with (Zhou et al., 2011) as Eq. (2) and (3).

$$C_p = C_{p1}\left(\frac{C_{p2}}{\lambda_i} - C_{p3}\cdot\beta - C_{p4}\cdot\beta^{C_{p5}} - C_{p6}\right)e^{\frac{-C_{p7}}{\lambda_i}} \tag{2}$$

$$\lambda_i = \frac{1}{\dfrac{1}{\lambda - C_{p8}\beta} - \dfrac{C_{p9}}{\beta^3 + 1}} \tag{3}$$

where C_{p1} to C_{p9} are the wind turbine constant coefficients of C_p.

The wind generator chosen for this study is a three-phase PMSG, where the mechanical torque (T_m) and electrical torque (T_e) can be calculated as (Lin et al., 2011)

$$T_m = \frac{P_m}{\omega_r} \tag{4}$$

$$T_e = \frac{P_e}{\omega_e} = \frac{2}{n_p}\frac{P_e}{\omega_r} \tag{5}$$

In general, the mechanical dynamic equation of a PMSG is given by

$$J\frac{d\omega_r}{dt} = T_m - B\omega_r - T_e \tag{6}$$

where ω_e and n_p are the electrical angular frequency and the number of poles, respectively. J is the moment of inertia of the wind turbine generator, and B is the friction coefficient of the generator.

The machine model of a PMSG in the rotor rotating reference frame can be described by (Lin et al., 2011)

$$v_q = Ri_q + p\lambda_q + \omega_s\lambda_d$$
$$v_d = Ri_d + p\lambda_d + \omega_s\lambda_d \quad (7)$$

and

$$\lambda_q = L_q i_q$$
$$\lambda_d = L_d i_d + L_{md} I_{fd} \quad (8)$$

$$\omega_s = n_p \omega_r \quad (9)$$

where v_d and v_q are the *d*-*q* axis stator voltages; i_d and i_q are the *d* and *q* components of stator currents; L_d and L_q are the *d*-*q* axis stator inductances; λ_d and λ_q are the *d*-*q* axis stator flux linkages; R is the stator resistance; ω_s is the inverter frequency; I_{fd} is the equivalent *d* component of magnetizing current; and L_{md} is the *d* component of mutual inductance.

2. HVDC

The HVDC link consists of an offshore, onshore VSC and dc cables. The VSCs of HVDC have the same structure. The wind turbine side VSC (WVSC) operated from the wind farms controls the voltage of offshore PCC bus. The power grid side VSC (GVSC) connected with onshore PCC bus is used primarily to maintain a constant voltage of the dc link. The reactive power exchanged at the two ac terminals is generated internally by the VSCs. The WVSC is responsible for collecting the power generated by the wind farm when the HVDC grid connection is used in the wind power generation system. The WFVSC is more like a stiff voltage source for the wind farm, and works as a slack node in the whole system as it automatically absorbs the power sending from the wind farm regardless of active or reactive power.

The GVSC is the key node for the wind power feeding into the gird system; its operational status will directly impact the grid power quality. The GVSC plays two roles in the operation of the whole system: one is to provide a robust dc voltage, which will be a strong backup support for the WVSC to provide a constant wind farm side bus voltage; another is to adjust the state of wind power feeding into the power grid. The dc transmission line current flows through the voltage source resulting in reactive and active power exchange with the ac system. The outer voltage and inner current loop of WVSC and GVSC can be converted in the *d*-*q* common reference frame as presented in (Zhou et al., 2011).

3. STATCOM External Control

The shunt STATCOM is like a synchronous compensator, with no inertia. The STATCOM can supply both the capacitive and the inductive compensation to support the bus voltage by independently controlling its output current. The real current is responsible for controlling the real power, while the reactive current is used to control the reactive power. It is also capable of improving the power system stability. The STATCOM generally is controlled by an external auxiliary control loops to damp the oscillations to improve the reference signal of the line voltage controller. The control structure of the STATCOM is shown in Fig. 2, where the typical external damping controller is which will be used for tests blown up in Fig. 3.

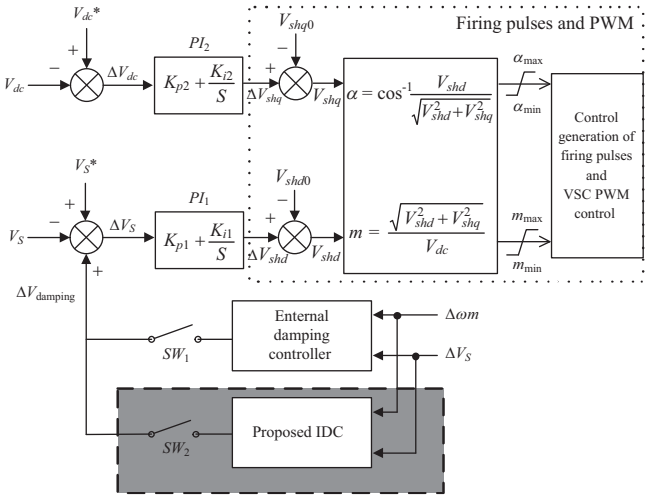

Fig. 2. The controller for the STATCOM.

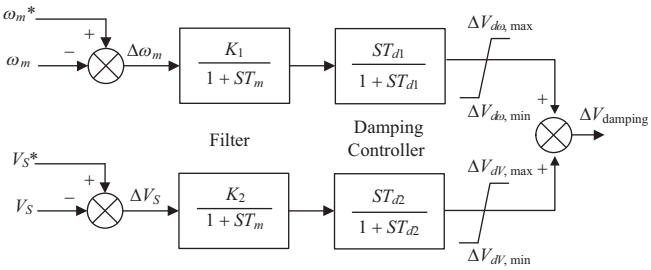

Fig. 3. External linear damping controller of the STATCOM.

V_S^* and V_{dc}^* are reference signals of the offshore PCC bus voltage and dc link voltage of STATCOM. K_{p1}, K_{p2}, K_{i1}, and K_{i2} are the proportional and integral gains of PI controllers, respectively. V_{shq0} and V_{shd0} are the initial values for the d-q axis voltages under synchronous reference frame. The direct and quadrature components of the voltages are then used to generate the modulation index m and phase shift α, which are then provided to the PWM generator to generate the gating signals for the power electronic switches in VSC.

The typical external damping controller of STATCOM in Fig. 3 is used as a baseline controller in this paper. It consists of the filter and damping controller. Since the wind turbine generator speed deviations are easier to obtain from measurement and analysis, the inputs of the damping loops are the generator speed deviation $\Delta\omega_m$ and the terminal voltage deviation ΔV_S related to the external controller. The main function of STATCOM is to regulate the line voltage at the point of connection, which can be used to damp the oscillations to improve the system stability. However, in various operating conditions of the power system, the performance of the linear external controller can be

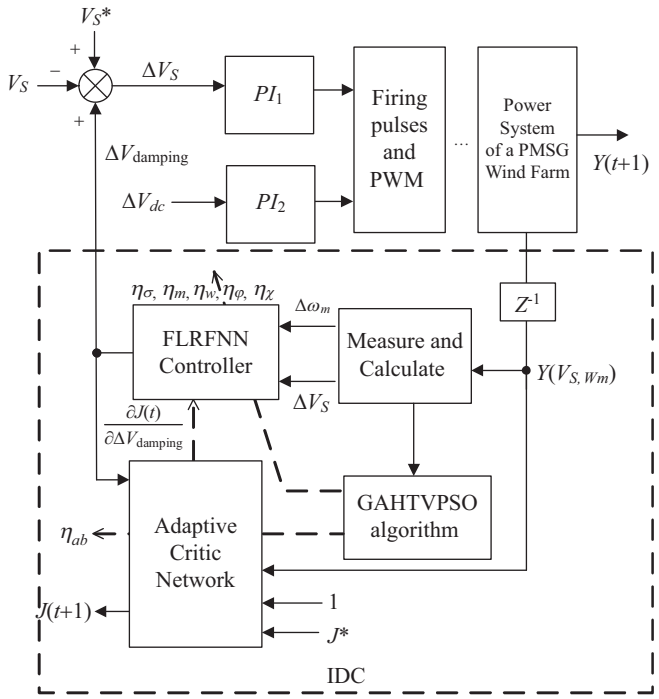

Fig. 4. IDC for STATCOM.

greatly affected by changes in the wind speed. To obtain the best performance of the power system, the controller parameters need fine-tuning at a single operating point.

III. DESIGN OF THE INTELLIGENT DAMPING CONTROLLER

The proposed IDC consists of three parts: the adaptive critic network, the FLRFNN and the GAHTVPSO algorithm, as shown in Fig. 4. The IDC input signal should be included in phase with the generator rotor speed deviation $\Delta\omega_m$ and the variation of terminal voltage ΔV_S. An FLNN is adopted to implement the function expansion for the FL-based RFNN to improve the accuracy of the function approximation. The adaptive critic network (Xu et al., 2013) is applied in order to provide suitable training signals for the FLRFNN controller. The configuration of the proposed FLRFNN and critic network is obtained by using the online tuning learning rates based on GAHTVPSO. The proposed IDC is capable of providing near optimal results for complex and uncertain nonlinear system in order to solve the Hamilton-Jacobi-Bellman equation of optimal control (Xu et al., 2013).

1. FLRFNN

Fig. 5 shows the design of the FLRFNN. It has an input layer, a membership layer with Gaussian function, a function expansion layer, recurrent fuzzy rule layer, output layer Membership layer and fuzzy rule layer are fed back to themselves through a time delay z^{-1}. There are 2 input variables, 10 membership nodes, 25 fuzzy rule nodes and 2 output nodes in this network,

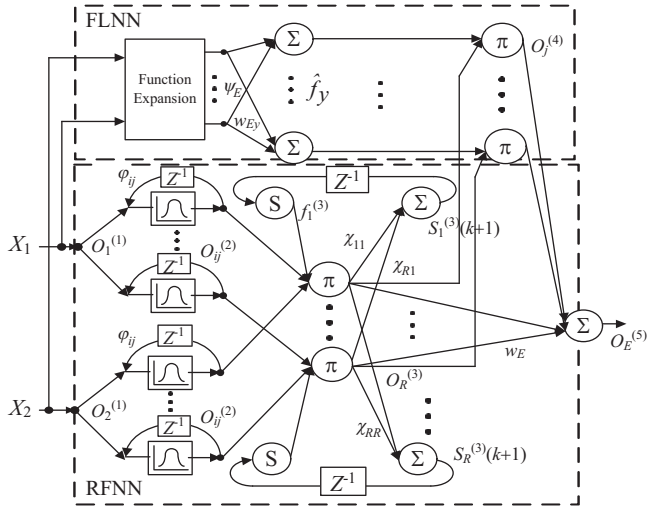

Fig. 5. FLRFNN controller.

where the number of nodes can be adjusted according to the knowledge of various applications.

The FLNN uses a feedforward neural network structure to generate a set of linearly independent functions, and functionally expands the elements of the input variables. The trigonometric function, the sine and cosine function is used in the FLNN, since it can be computed more quickly than the Gaussian. Moreover, it also provides better performance when the outer product term is taken into account in the function expansion (Lin et al., 2010; Wang and Sa-Nguyen Thi, 2013).

The input vector $\boldsymbol{X} = [X_1, X_2]^T$ is a functional expansion that uses a trigonometric polynomial basis function, and can be written in the enhanced space as $\boldsymbol{\psi_E} = [\psi_1, \psi_2, \ldots \psi_p] = [1, X_1, \sin(\pi X_1), \cos(\pi X_1), X_2, \sin(\pi X_2), \cos(\pi X_2), X_1X_2]$, where X_1X_2 is the outer product term. Furthermore, the FLNN output is expressed by a linear sum of the yth node as

$$\begin{aligned} \hat{f}_y(k) &= \theta\left(\sum\nolimits_E \psi_E(x_i)\cdot w_{Ey}\right) \\ &= \theta\left(w_{Ey}\cdot\psi_E(\boldsymbol{X})\right), \\ E &= 1, 2, \ldots, 9 \text{ and } y = 1, 2, \ldots, 9 \end{aligned} \tag{10}$$

where $\hat{f}_y$ is the outer product term. w_{Ey} is the connective weight, and ψ_E is the function expansion output. θ is a set of basic functions. The network input $\boldsymbol{X} = [\Delta\omega_m, \Delta V_S]^T$ is used and FLRFNN can employ the neurons to increase dynamic characteristics of the network.

The RFNN can retain dynamic characteristics of the network through trainings of the weights φ_{ij} and χ_{RR}, and has a better dynamic response than that of the general RFNN. O is the output of each layer, with superscripts to represent the layer-number and subscripts to represent the signal number and are given as

$$O_i^{(1)}(t) = X_i^{(1)}(t) \quad i = 1, 2 \tag{11}$$

$$O_{ij}^{(2)}(k)=\exp\left\{-\frac{\left(O_i^{(1)}(k)+O_{ij}^{(2)}(k-1)\cdot\varphi_{ij}-m_{ij}\right)^2}{\left(\sigma_{ij}\right)^2}\right\} \quad (12)$$

$$f_R(k)=\frac{1}{1+\exp(-S_R)} \quad (13)$$

$$O_R^{(3)}(k)=f_R\cdot\Pi_{i=1}^{2}O_{ij}^{(2)}(k)\cdot w_{ij} \quad (14)$$

$$O_j^{(4)}(k)=\Pi O_R^{(3)}(k)\cdot\hat{f}_y(k) \quad (15)$$

$$O_E^{(5)}(k)=\frac{\sum_{R=1}^{p}O_R^{(3)}(k)\hat{f}_y(k)}{\sum_{R=1}^{p}w_E O_R^{(3)}(k)} \quad (16)$$

where k denotes the iteration number of FLRFNN. m_{ij} is the Mean, σ_{ij} is the Standard Deviation (STD) of the i-term input linguistic variable $O_i^{(1)}$ in the j-term. $R \in \{1, 2, 3 \ldots, \mathrm{j}\times\mathrm{j}\}$; $w_E = w_{ij} = 1$; χ_{RR} is the recurrent weight. The parameters of the FLRFNN to be trained are σ_{ij}, m_{ij}, w_{Ey}, φ_{ij} and χ_{RR}. $O_E^{(5)}$ is called an output linguistic node, which performs the operation of defuzzification. $O_E^{(5)} = \Delta V_{\text{damping}}$, which is added to the voltage reference V_s* of the PI_1 controller (Fig. 4).

2. Adaptive Critic Network

An adaptive critic network can be designed to identify the sensitivity use of FLRFNN $\partial J/\partial\Delta V_{\text{damping}}$ to learn the cost-to-go associated with the power system. This ability is of great importance for real time optimal control operations when there are changes in configuration and operating conditions. The cost-to-go function J of Bellman's equation of dynamic programming estimated by the critic network is (Wang and Sa-Nguyen Thi, 2013).

$$\begin{aligned}J(t)&=\sum_{k=0}^{\infty}\gamma^k U\left(t+k\right)\\&=U\left(t\right)+\sum_{k=0}^{\infty}\gamma^k U\left[\left(t+1\right)+k\right]\\&=U\left(t\right)+\gamma\cdot J\left(t+1\right)\end{aligned} \quad (17)$$

where the utility function $U(t)$ is an important factor to form the optimal cost-to-go γ represents the discount factor (0-1). The utility function of the critic network includes U_a(t) and U_b(t) is

$$U\left(t\right)=U_a(t)+U_b(t) \quad (18)$$

$$U_a(t)=\left|\Delta\omega_m(t)+\Delta\omega_m(t-1)+\Delta\omega_m(t-2)\right| \quad (19)$$

$$U_b(t)=\left|\Delta V_S(t)+\Delta V_S(t-1)+\Delta V_S(t-2)\right| \quad (20)$$

The node output of each layer of the critic network and the

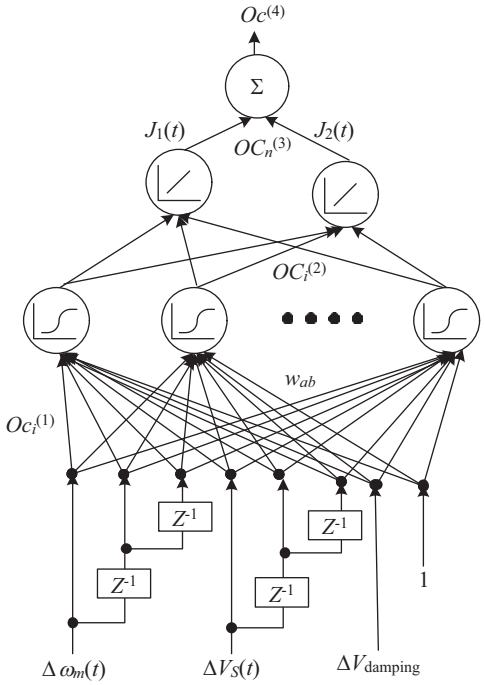

Fig. 6. Adaptive critic network.

superscripts represent the layer-number of the output Oc, while the subscripts present the signal number of the related output, and are given as

$$\begin{aligned}&Oc_i^{(1)}(t)=F_i^{(1)}(t),\ i=1,\ldots,8\\&F_i=\left[\Delta\omega_m(t)+\Delta\omega_m(t-1),\ldots,\Delta V_S(t-2),\Delta V_{\text{damping}},1\right]\end{aligned} \quad (21)$$

$$Oc_i^{(2)}(t)=\frac{1}{1+\exp^{H}},\ H=\sum_{i=1}^{8}Oc_i^{(1)}\cdot w_{ab} \quad (22)$$

$$Oc_n^{(3)}(t)=J_n(t)=\sum_{n=1}^{2}Oc_i^{(2)},\ n=1,2 \quad (23)$$

$$Oc^{(4)}(t)=\sum Oc_n^{(3)}=J(t) \quad (24)$$

where w_{ab} is the connecting weights of the input layer to hidden layer.

Using Eqs. (19) and (20), the STATCOM should improve the performance of both generator speed deviation $\Delta\omega_m$ and PCC voltage deviation ΔV_S. The adaptive critic network in Fig. 6 has a four-layer feed-forward network structure. The training process ensures that the critic network provides optimal control to minimize the $J(t)$, which enables the FLRFNN controller to provide the optimal damping control signal to the STATCOM in this paper.

3. The Training Process of FLRFNN and Adaptive Critic Network

The gradient descent algorithm with the mean squared error

function as the error function E can be defined by (Wang and Sa-Nguyen Thi, 2013).

$$E = \frac{1}{2}[J^*(t) - J(t)]^2 = \frac{1}{2}[U(t) + \gamma \cdot J^*(t+1) - J(t)]^2 \tag{25}$$

where $J^*(t)$ is the reference value of the cost-to-go, which is zero in the case of dealing with deviation signals.

The BPTT can be used to find the estimates of the gradient (Xu et al., 2013). In order to use an on-line algorithm for the critic network and the proposed FLRFNN, the error term of critic network δ_{ab} can be analyzed. The feed-forward part of error terms of FLRFNN, δ_{FLRFNN}^{fed} based on the chain rule can be represented as (26) and (27). The recurrent error term, δ_{FLRFNN}^{rec} of FLRFNN can be propagated and unfolded for more than two layers for capturing previous information. δ_{FLRFNN}^{rec} can be represented as Eq. (28)

$$\delta_{ab} = \sum_{i=1}^{8} \frac{\partial E}{\partial w_{ab}} = \sum_{i=1}^{8} \frac{\partial E}{\partial J} \cdot \frac{\partial J}{\partial w_{ab}} \tag{26}$$

$$\delta_{FLRFNN}^{fed} = \sum_{u}^{n} \frac{\partial E}{\partial W_{FLRFNN}^{fed}} = \sum_{u}^{n} \frac{\partial E}{\partial J} \cdot \frac{\partial J}{\partial V_{\text{damping}}} \cdot \frac{\partial V_{\text{damping}}}{\partial W_{FLRFNN}^{fed}} \tag{27}$$

$$\delta_{FLRFNN}^{rec}(t-1) = \sum_{j}^{n} \frac{\partial E}{\partial W_{FLRFNN}^{rec}} = \sum_{j}^{n} \frac{\partial E}{\partial J} \cdot \frac{\partial J}{\partial V_{\text{damping}}} \cdot \frac{\partial V_{\text{damping}}}{\partial W_{FLRFNN}^{rec}} \tag{28a}$$

where $\frac{\partial J}{\partial \Delta V_{\text{damping}}}$ is the sensitivity of FLRFNN by the critic network identified as

$$\frac{\partial J}{\partial \Delta V_{\text{damping}}} = \frac{\partial J}{Oc^{(4)}} \cdot \frac{Oc^{(4)}}{Oc_n^{(3)}} \cdot \frac{Oc_n^{(3)}}{Oc_i^{(2)}(t)} \cdot \frac{Oc_i^{(2)}(t)}{\partial \Delta V_{\text{damping}}} \tag{28b}$$

The formula for adjusting the w_{ab} of the critic network, weights W_{FLRFNN}^{fed} and W_{FLRFNN}^{rec} of FLRFNN are shown in (29)-(31). More details of the training procedure can be found in an earlier work (Jaeger, 2013).

$$w_{ab}(t+1) = w_{ab}(t) - \eta_{ab} \cdot Oc_i^{(2)}(t) \cdot \delta_{ab}(t) \tag{29}$$

$$\delta_{FLRFNN}^{fed}(t+1) = \delta_{FLRFNN}^{fed}(t) - \eta_{FL} \sum_{\tau=0}^{T} O^{(l)}(t-\tau) \cdot \delta_{FLRFNN}^{fed}(t-\tau) \tag{30}$$

$$\delta_{FLRFNN}^{rec}(t+1) = \delta_{FLRFNN}^{rec}(t) - \eta_{\varphi} \sum_{\tau=0}^{T} O_{ij}^{(2)}(t-\tau-1) \cdot \delta_{FLRFNN}^{rec}(t-\tau) \tag{31}$$

where $W_{FLRFNN}^{fed} = \left[\sigma_{ij}, m_{ij}, w_{Ey}, \chi_{RR}\right]$ and $W_{FLRFNN}^{rec} = \varphi_{ij} \cdot \eta_{ab}$ is the learning rate of w_{ab}. $\eta_{FL} = \left[\eta_{\sigma}, \eta_m, \eta_w, \eta_{\chi}\right]$ and η_{φ} are the learning rates of weights of feed-forward and recurrent part of FLRFNN. i is the layer 2 number of critic network. n is the number of training samples. u is the own number of every layer units of FLRFNN. τ is an arbitrary number of time steps in unfolded recurrent layer of FLRFNN. T is the total unfolded number of FLRFNN. $O^{(1)}$ is the output number of ever layers (l = 1-5) of FLRFNN.

The learning rates η_{σ}, η_m, η_w, η_{φ}, η_{χ} and η_{ab} of IDC should be properly set in the BPTT algorithm. A relatively large or small learning rate may affect the progress of BPTT algorithm, and even lead to failure of the learning process. This paper thus uses the GAHTVPSO to find the optimal values of these parameters to improve the learning capability.

4. Learning Rates Adjustment Using GAHTVPSO

To further improve the online learning ability of the IDC, the GAHTVPSO algorithm is used to tune the learning rates η_{σ}, η_m, η_w, η_{φ}, η_{χ} and η_{ab}. In the GAHTVPSO, each particle adjusts its position according to its own experience and those of its neighbors, including the current velocity, position, and the best previous position experienced by itself and its neighbors.

Two pseudo-random sequences r_1~U(0, 1) and r_2~U(0, 1) are used to simulate the stochastic nature of the algorithm. For all dimensions d, let R_i^{d} and $pbest_i^{\text{d}}$ be the current position and current personal best position. The velocity update law is shown in (32). In addition, the inertia weight is set at $\omega = 0$. GAHTVPSO can reduce a parameter setting the acceleration coefficients c_1 and c_2 can be modified by Eqs. (33) and (34) (Jaeger, 2013). These settings are called the time-varying acceleration coefficients.

$$v_i^d(N+1) = \omega v_i^d(N) + c_1 \cdot r_1 \cdot \left(pbest_i^d - R_i^d(N)\right) + c_1 \cdot r_2 \cdot \left(pbest_i^d - R_i^d(N)\right) \tag{32}$$

$$c_1 = \left(c_{1f} - c_{1i}\right) \cdot \frac{N}{N_{\max}} + c_{1i} \tag{33}$$

$$c_2 = \left(c_{2f} - c_{2i}\right) \cdot \frac{N}{N_{\max}} + c_{2i} \tag{34}$$

$$R_i^d(N+1) = R_i^d(N) + v_i^d(N+1) \tag{35}$$

Table 1. The Parameters and initial values of test system.

PMSG-based OWF and transmission line
S = 100MW; 3.75 A; 3000 r/min, ρ = 1.25 kg/m^3; r = 0.5 m; J = 1.32 × 10^{-3} Nms^2, B = 5.78 × 10^{-3} Nm s/rad, T_w= 0.69/24 kV, R_t = 0.02 p.u., X_t = 0.08 p.u.
STATCOM with control system
$S_{STATCOM}$ = 70 MVA, frequency = 60 Hz, R_s = 0.04 Ω, L_s = 0.0001 H, K_{p1} = 0.0015, K_{p2} = 0.0015, K_{p1} = 0.001, K_{i1} = 0.15, K_{i2} = 0.1, C_{dc} = 0.6 p.u.
HVDC
Rated power of WVSC and GVSC = 100 MVA, V_{dc1} = V_{dc2} = 150 kV, C_{dc1} = C_{dc2} = 0.6 p.u., Xf_1 = Xf_2 = 0.2 p.u,
IDC
P = 15, d = 5, initial learning rates η_σ = 0.95, η_m = 0.815, η_w = 0.8, η_φ = 0.79, η_χ = 0.6, c_{1f} = c_{2f} = c_{1i} = c_{2i} = 1, $c3$ = 1, β = 0.1, α = 0.1

where v_i^d and R_i^d are the current velocity and position of the particle. $N_{\max}$ is the maximum number of iterations.c_{1i} and c_{2i} are the initial parameter settings, while c_{1f} and c_{2f} are the final parameter settings.

Step 1: Define the Basic Conditions

With R_i^d= [R_1, R_2, R_3, R_4, R_5, R_6] for the learning rates (η_σ, η_m, η_w, η_φ, η_χ and η_{ab}), the population size is set to P = 15, and the dimensionality of the particle is set to d = 6. The parameters need to be optimized within minimum and maximum ranges.

Step 2: Initialize the Location and Velocity

The initial locations $R_i^d(N)$ and velocities $v_i^d(N)$ of all the particles are randomly generated in the search space. The initial *pbest* of a particle is set at its current position and the *gbest* of a group is selected from among the *pbests*. The elements in vector $R_i^d(N)$ are randomly generated by

$$R_i^d \sim U\left[\eta_{\min}^d, \eta_{\max}^d\right] \tag{36}$$

where $U\left[\eta_{\min}^d, \eta_{\max}^d\right]$ designates the outcome of a uniformly distributed random variable ranging over the given lower and upper bounded values $\eta_{\min}$ and $\eta_{\max}$ of the learning rate.

Step 3: Determination of the Fitness Function

For each vector R_i^d, a fitness value should be assigned and evaluated. In this paper, a suitable fitness function is selected to calculate the fitness value as

$$FIT = \frac{1}{0.1 + abs\left(\omega_m - \omega_m^*\right) + abs\left(V_S - V_S^*\right)} \tag{37}$$

where *FIT* is the fitness value, and *abs*(·) is the absolute function. 0.1 is added to the dominant part to avoid approaching infinity.

Step 4: Selection of Pbest and Gbest

Each particle R_i^d memorizesits own fitness value and chooses the maximum one that is the best so far as $pbest_i^d$. The maximum vector in the population $pbest_i^d = \left[pbest_1^d, pbest_2^d, \ldots, pbest_p^d\right]$ is then obtained. Moreover, each particle R_i^d is set directly to $pbest_i^d$ in the first iteration, and the particle with the best fitness value among the various *pbest* is set to be the global best *gbest*.

Step 5: Check the Gbest for Updates:

If *gbest* has not changed for some designated steps, crossover operation is performed on *gbest* using a GA chromosome. The reorganization of the position and velocity are carried out by

$$R_i^d(N+1) = c_3 \cdot rand(\cdot) \cdot \left(gbest_i^d - R_i^d(N)\right) \tag{38}$$

$$\begin{cases} p_{child1} = \beta p_{parent1} + (1-\beta) p_{parent2} \\ p_{child2} = \beta p_{parent2} + (1-\beta) p_{parent1} \end{cases} \tag{39}$$

$$\begin{cases} v_{child1} = \dfrac{v_{parent1} + v_{parent2}}{\left|v_{parent1} + v_{parent2}\right|} \cdot \left|v_{parent1}\right| \\ v_{child2} = \dfrac{v_{parent1} + v_{parent2}}{\left|v_{parent1} + v_{parent2}\right|} \cdot \left|v_{parent2}\right| \end{cases} \tag{40}$$

where c_3 is the weighting factor of the stochastic acceleration, and *rand*() represents a uniform random number between 0 and 1. p_{parent} and p_{child} are the parent and child generations of the position. v_{parent} and v_{child} are the parent and child generations of the velocity. β represents the interpolation value between the parent and child generations, and this is a uniform random number between 0 and 1.

Step 6: Update Velocity and Position

The new velocity is then added to the current position of the particle to obtain its next position using Eq. (32) and Eq. (35).

Step 7: Check Convergence

Steps 3-6 are repeated until the best fitness for *gbest* is obtained or a set number of generations are reached. The final

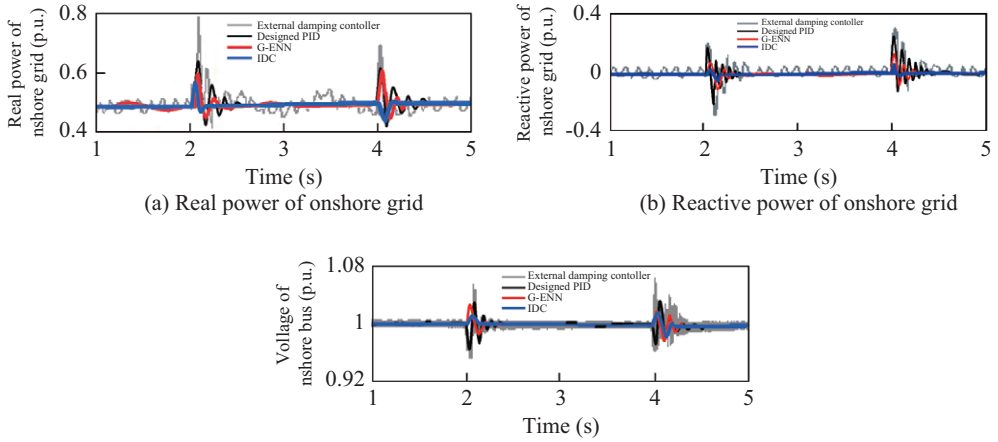

(a) Real power of onshore grid

(b) Reactive power of onshore grid

(c) PPC bus voltage of onshore grid

Fig. 7. The responses of stability of changes for onshore grid voltage.

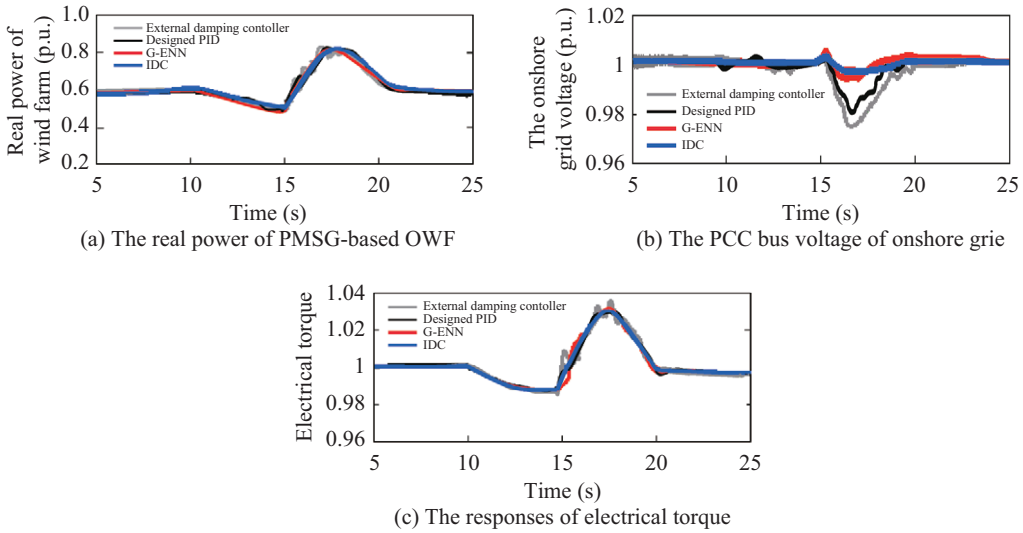

(a) The real power of PMSG-based OWF

(b) The PCC bus voltage of onshore grie

(c) The responses of electrical torque

Fig. 8. The stability of changes in wind speed.

$pbest_i^d$ is the optimal learning rate (η_σ, η_m, η_w, η_φ, η_χ and η_{ab}) of IDC.

IV. CASE STUDIES AND SIMULATION RESULTS

Many tests were carried out to test the IDC. The OWF with HVDC in Fig. 1 was built in a PSCAD/EMTDC environment. The FLRFNN and critic network with GAHTVPSO were implemented in MATLAB. The parameters and initial values of the system are shown in Table 1. The optima capacity and location of STATCOM is determined by search algorithms in (Lin et al., 2009). To check the effectiveness of the proposed IDC, it is compared with the external linear damping controller, the PID damping controller (Mitra et al., 2011) and the Grey-Elman Neural Network (G-ENN) (Lin et al., 2013), with the parameters used in this work being taken from the references.

Case 1. Single-Machine Infinite-Bus (SMIB) System

The wind speed is assumed to be 14 m/s and the onshore grid voltage decreases 20% at 2nd second and increases 20% at 4th second. Figs. 7(a)-(c) shows the dynamic responses and the proposed shows a better performance. It also shows that IDC has a better transient stability for both real and reactive powers. Fig. 7(c) shows the capability of IDC to regulate the bus voltage. The methods can fast support the onshore grid voltage at 1 p.u.

Case 2. Sudden Wind Change Test

Figs. 8 show the stability of dynamic responses when the wind speed changes from 14 m/s to 11 m/sat the 10th second, from 10 m/s to 19 m/s at the 15th second and from 19 m/s to 14 m/s at the 17th second. Fig. 8(a) shows that the smallest amplitude changes for real powers can be obtained with for IDC. Similarly,

Table 2. Results for Several Methods.

Method	Interactive Number	CPU Time (sec)	Mean Square Error (10^{-3})	Accuracy (%)
GAHTVPSO	37	1.48	1.23	98.77
MPSO	33	1.32	4.36	95.64
IPSO	57	2.28	5.08	94.92
Fuzzy	98	3.92	12.35	87.65

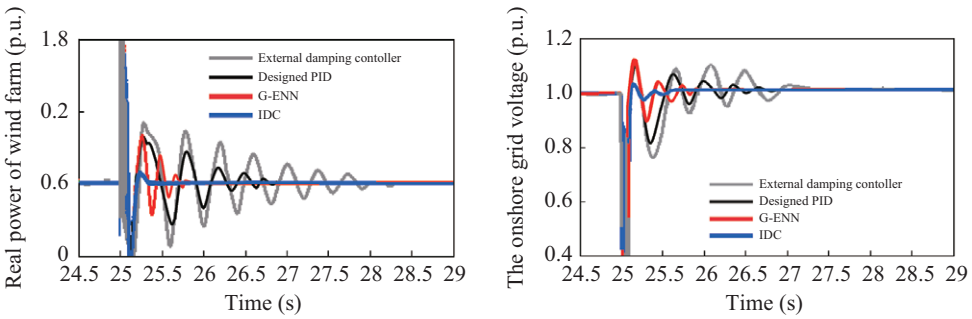

(a) The real power of PMSG-based OWF

(b) The PCC bus voltage of onshore grie

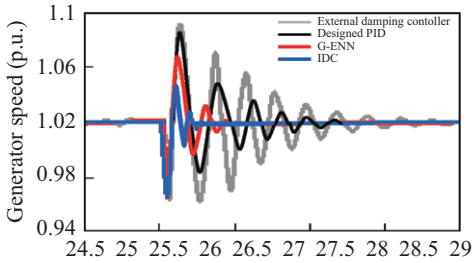

(c) The generator speed

Fig. 9. The transient stability of the three phase fault.

Fig. 8(b) show that magnitudes change. It can be clearly seen that when the designed IDC is combined with the STATCOM, the PCC voltage can have the smallest variations onshore bus voltage are regulated to 1 p.u. The dynamic responses in damping out the electrical torque oscillations in the wind turbine are shown in Fig. 8(c). The results show that the proposed IDC is better than external linear damping controller, designed PID damping controller and the G-ENN, and can produce the smallest variations. However, the power oscillation is effectively mitigated and the system stability is improved with either one of the damping options.

Case 3. Damping for Faults

A three-phase fault is simulated at the 25th second and is cleared at 25.1th second. Fig. 9(a) shows that IDC has a better damping effect and a faster convergence rate than others. The fault causes large fluctuations in the temporary voltage. Figs. 9(b) shows that IDC can effectively improve the onshore bus voltage transient stability. A faster voltage recovery is achieved bus voltage. Fig. 9(d) show that the rotor speed of the PMSG can recover more quickly to steady states.

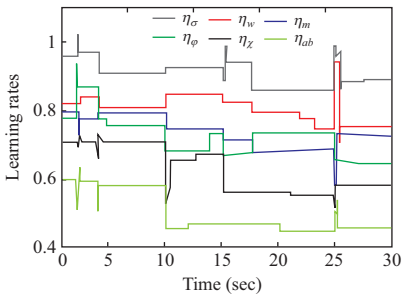

Fig. 10. The learning rates of FLRFNN and the critic network.

Case 4. Learning Rates of GAHTVPSO Test

The learning rates of FLRFNN and the critic network are shown in Fig. 10. Using the online tuning learning rates based on GAHTVPSO, the results can be optimized for the proposed IDC when uncertainties occur. In addition, comparisons with four other PSO algorithms (21-22) are given in Table 2. From Table 2, we can see that GAHTVPSO has the best accuracy and has a faster convergence rate than other PSO approaches.

Fig. 1

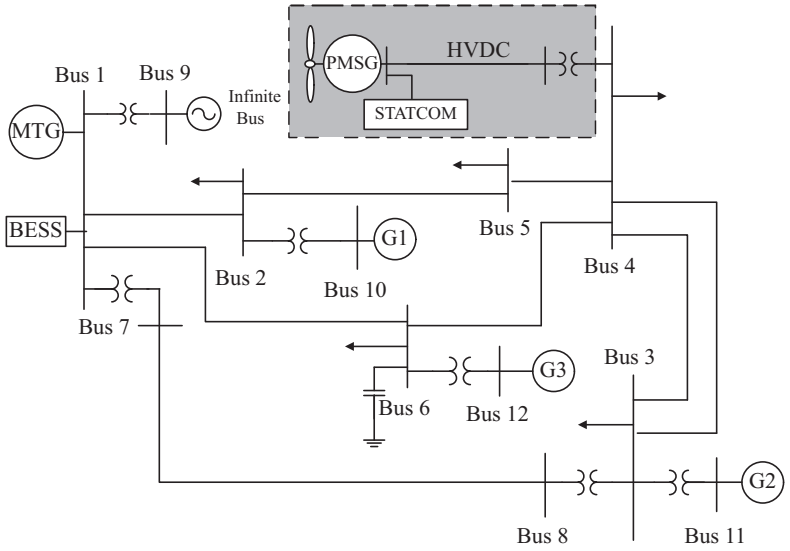

Fig. 11. The IEEE benchmark 12-bus hybrid multi-machine system.

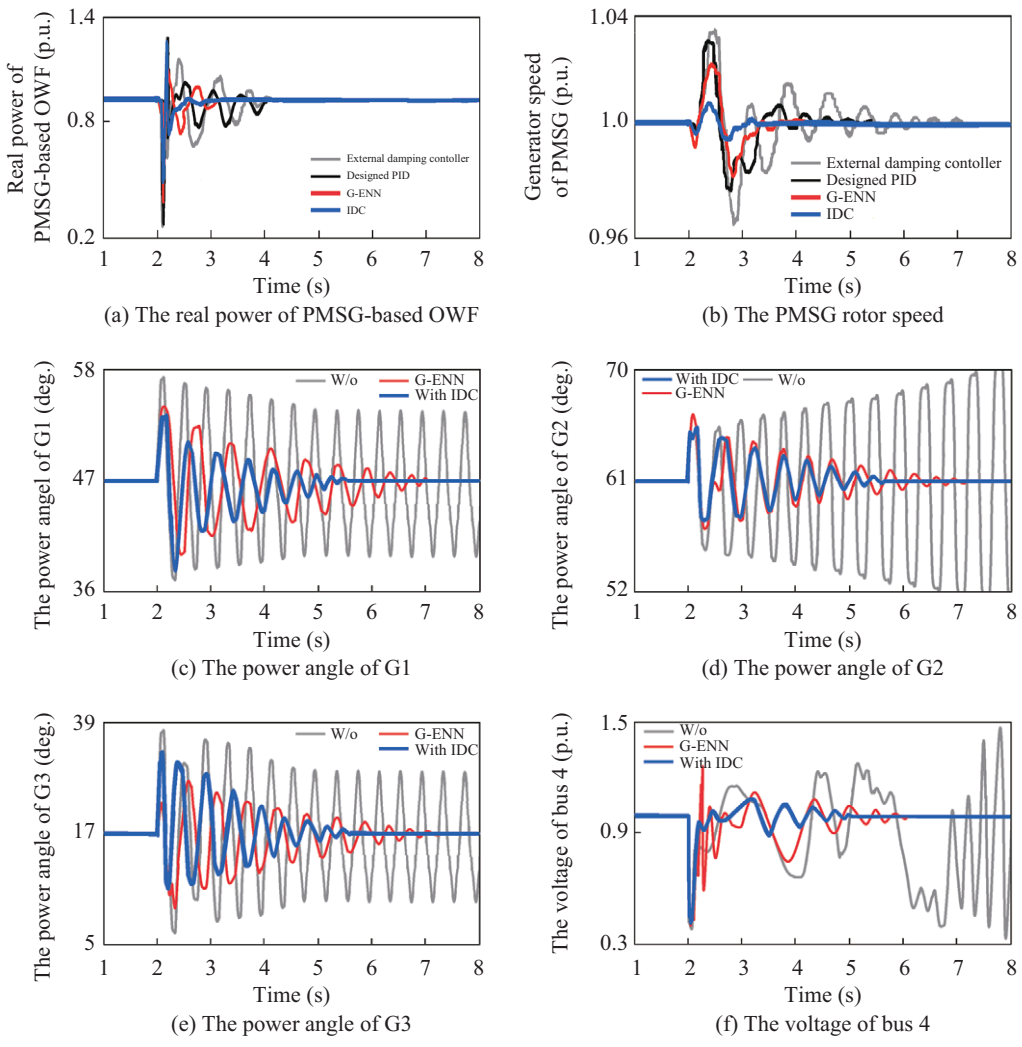

(a) The real power of PMSG-based OWF
(b) The PMSG rotor speed
(c) The power angle of G1
(d) The power angle of G2
(e) The power angle of G3
(f) The voltage of bus 4

Fig. 12. The transient stability of the three phase fault.

Case 5. Multi-Machine System Test

In this case, the IEEE benchmark 12 bus hybrid multi-machine system (Mitra et al., 2011) is used for test consisting of three power generation systems, 12 buses, a BESS and a micro-turbine generations (MTG) as shown in Fig. 11. The OWF through a HVDC link with the STATCOM in Fig. 1 is connected to the multi-machine system at bus 4. The wind speed is assumed to be 19 m/s and a fault is simulated at 2th second for a duration of 100ms at bus 4. Fig. 12(a) shows the real power of PMSG-based OWF connected to the multi-machine system. The dynamic responses are shown in Figs. 12(b)-(d). It can be seen that with IDC the generators rotor speed of G1-G3 and PMSG can recover more quickly to the steady state around 2.8 and 3.3 second.

A three-phase fault at bus 4 and bus 2 were simulated to test the system limit. The fault is simulated at 2th and cleared after 100 ms. Figs. 12(f) shows the bus 4 voltage. It shows that the proposed IDC can effectively improve the bus 4 voltage within a few cycles and damps out the power angle oscillations around 5 and 5.5 second while other controllers could not achieve.

V. CONCLUSION

This paper demonstrated the effectiveness of the proposed IDC for STATCOM in damping out the oscillations of the OWF. The adaptive critic network uses the FLRFNN controller to provide the optimal damping control signal to the STATCOM, and GAHTVPSO algorithm is used to improve the learning rates on line. The results of the simulations show that this approach can effectively stabilize the network under faults. The proposed STATCOM damping controller mitigates the oscillations and can also solve the problem of power stability.

REFERENCES

Cardenas, R., R. Pena, J. Proboste, G. Asher and J. Clare (2005). MRAS observer for sensorless control of standalone doubly fed induction generators. IEEE Transactions on Energy Conversion 20, 710-718.

Chaturvedi. K. T., M. Pandit and L. Srivastava (2008). Self-organizing hierarchical particle swarm optimization for nonconvex economic dispatch. IEEE Transactions on Power System 23, 1079-1087.

Chen, C. H., C. T. Lin and C. J. Lin (2007). A functional-link-based fuzzy neural network for temperature control. IEEE Symposium on Foundations of Computational 53-58.

Chen, W. L., W. G. Liang and H. S. Gau (2010). Design of a mode decoupling STATCOM for voltage control of wind-driven induction generator systems. IEEE Transactions on Power Delivery 25, 1758-1767.

Eberhart, R. C. and Y. Shi (2001). Particle swarm optimization: Developments, applications and resources.

George, N. V. and G. Panda (2012). A Particle- swarm- optimization- based decentralized nonlinear active noise control system. IEEE Transactions on Instrumentation and Measurement 61, 3378-3386.

Hong, Y. Y. and Y. F. Luo (2009). Optimal VAR control considering wind farms using probabilistic load-flow and gray-based genetic algorithms. IEEE Transactions on Power Delivery 24, 1441-1449.

Jaeger, H. (2013). A tutorial on training recurrent neural networks, covering BPTT, RTRL, EKF and the 'Echo State Network' approach. GMD Report 159, German National Research Center for Information Technology, German, 15, 1-46.

Lin, F. J., L. T. Teng, J. W. Lin and S. Y. Chen (2009). Recurrent functional-link-based fuzzy- neural- network-controlled induction-generator system using improved particle swarm optimization. IEEE Transactions on Industrial Electronics 56, 1557-1577.

Lin, W. M., C. M. Hong and T. C. Ou (2010). MRAS-based sensorless wind energy control for wind generation system using RFNN. Proceeding of IEEE Conference on Industrial Electronics and Applications, Taichung, Taiwan, Republic of China 2270-2275.

Lin, W. M., C. M. Hong, C. H. Huang and T. C. Ou (2013). Hybrid control of a wind induction generator based on grey-elman neural network. IEEE Transactions on Control Systems Technology 21, 2367-2373.

Lin, W. M., C. M. Hong, T. C. Ou and T. M. Chiu (2011). Hybrid intelligent control of PMSG wind generation system using pitch angle control with RBFN. Energy Conversion and Management. 52, 1244-1251.

Lin, W. M., K. H. Lu, C. H. Huang, T. C. Ou and Y. H. Li (2009). Optimal Location and Capacity of STATCOM for Voltage stability Enhancement using ACO plus GA. Proceeding of International Conference of Advanced Intelligent Mechatronics, Singapore, 1915-1920.

Lingling, F. and M. Zhixin (2012). Mitigating SSR using DFIG-based wind generation. IEEE Transactions on Sustainable Energy 3, 349-58.

Mitra, P., G. K. Venayagamoorthy and K. Corzine (2011). Smart park as a virtual STATCOM. IEEE Transactions on Smart Grid 2, 445-455.

Mohagheghi, S., G. K. Venayagamoorthy and R. G. Harley (2007). Optimal neuro-fuzzy external controller for a STATCOM in the 12-bus benchmark power system. IEEE Transactions on Power Delivery 22, 2548-2558.

Proceeding of IEEE Conference of Congress on Evolutionary Computation, Seoul, South Korea, 81-86.

Varshney, S., L. Srivastava and M. Pandit (2011). Optimal location and sizing of STATCOM for voltage security enhancement using PSO-TVAC. Proceeding of IEEE International Conference on Power and Energy Systems, Chennai, India, 22-24.

Wai, R. J., S. Cheng, Y. F. Lin and Y. C. Chen (2014). Installed capacity selection of hybrid energy generation system via improved particle- swarm-optimization. IET. Generation, Transmission & Distribution 8, 742-752.

Wang, L. and M. Sa-Nguyen Thi (2013c). Stability enhancement of a pMSG-based offshore wind farm fed to a multi- machine system through an LCC-HVDC link. IEEE Transactions on Power System. 28, 3327-3334.

Wang, L. and D. N. Truong (2013). Dynamic Stability Improvement of Four Parallel-Operated PMSG-Based Offshore Wind Turbine Generators Fed to a Power System Using a STATCOM. IEEE Transactions on Power Delivery 28, 111-119.

Wang, L. and D. N. Truong (2013a). Stability enhancement of DFIG-based offshore wind farm fed to a multi-machine system using a STATCOM. IEEE Transactions on Power System 28, 2882-2889.

Wang, L. and D. N. Truong (2013b). Comparative stability enhancement of PMSG-based offshore wind farm fed to an SG-based power system using an SSSC and an SVeC. IEEE Transactions on Power System 28, 1336-1344.

Xu, X., Z. Hou and C. Lian (2013). Online learning control using adaptive critic designs with sparse kernel machines. IEEE Transactions on Neural Networks and Learning Systems 24, 762-775.

Yang, S. H. and J. F. Kiang (2014). Optimization of asymmetrical difference pattern with memetic algorithm. IEEE Transactions on Antennas and Propagation 62, 2297-2302.

Zhou, H., G. Yang and J. Wang (2011b). Modeling, analysis, and control for the rectifier of hybrid HVdc Systems for DFIG-based wind farms. IEEE Transactions on Energy Conversion 26, 340-53.

Zhou, H., G. Yang, J. Wang and H. Geng (2011a). Control of a hybrid high-voltage DC connection for large doubly fed induction generator-based wind farms. IET Renewable Power Generation 5, 36-47.